Morphology and Geomagnetic Effects of Corotating Interaction Regions in 2008 - 2014

DarijeMaričić[1], Dragan Roša[1], Filip Šterc[1] and Mile Karlica[2]

[1] Zagreb Astronomical Observatory , Croatia.
[2] Sapienza University of Rome, Italy.

Abstract

We presented an analysis of the geoeffectiveness of corotating interaction regions (CIRs) employing the data recorded from January 2008 to December 2014. For this purpose we made a list of 283 solar wind (SW) disturbances incorporated into an online catalog for general use. After we separated solar wind signatures on: CIRs, interplanetary coronal mass ejections (ICMEs), interactions and complex signatures; we focused our attention on 173 CIRs (61% of all SW signatures) where the stream interface (SI) was clearly recognizable. Furthermore, we analyzed in detail the correlation of solar wind parameters in different parts of CIRs, particularly in front and behind of SI, with changes in geoeffectiveness. In this analysis, in most events (95% of the analyzed CIRs) weak increase of Dst index occurs between forward shock and SI, while the main decreases of Dst index occurs between SI and reverse shock of CIR. The correlation coefficients between Dst index and the magnetic field B, proton density Np, flow speed v and proton thermal speed v_{th}, in the region behind the SI are: cc = 0.72, 0.62, 0.45 and 0.64, respectively. Correlations for region between forward shock and SI are significantly lower.

Keywords*: Sun, coronal mass ejection, solar wind disturbance, stream interface, corotating interaction regions*

Introduction

Corotating interaction regions (CIRs) are formed by interaction of the high speed solar wind streams (HSSs), with velocity up to 900 kms^{-1} and slow solar wind stream with typically velocity of ~ 400 kms^{-1} (e.g., *Tsuratani et al.,* 2006, and references therein). Since CIRs originates from a coronal hole, they cause recurrent activity in the interplanetary space (e.g. *Gosling,* 1996). CIRs at heliocentric distance of around 1 AU are usually bounded by magnetohydrodinamic forward and reverse waves, who develop into forward and reverse shocks at a larger distance, occasionally in some events already at 1 AU (*Smith and Wolfe,* 1976). CIRs causes periodic geomagnetic storms of weak to medium strenghts (e.g. *Vennerstorm,* 2001; *Verbanec et al.,* 2011a,b; *Hajra et al.,* 2013, *Vršnak et al.,* 2017). Although this phenomena is much stronger when it is caused by a single ICME or with interaction of ICMEs, the importance of CIRs is that they occur more common throughout the

solar cycle and their cumulative effect is larger than those of ICMEs (*Tsuratani et al.,* 2006). From the measurements of the solar wind at 1 AU, CIR structure is characterized by compression region associated with stream interface (SI). Inside the compression region the magnetic field, the temperature and the plasma density are increased (*Dumbović et al.*, 2012, and references therein). Compression region usually lasts typically one day. The whole region contains strong fluctuation and the increase of the southward-directed magnetic field is always present. Fast HSS from coronal holes lasts typically several days and attain flow speeds that can reach values above 800 kms^{-1}. For the evolution and structure of CIRs see articles *Baloghet al.,* 1999 as well as *Gosling and Pizzo,* 1999. The main objective of the analysis presented in this article is a comparison of geoeffectiveness caused by different parts of the CIR, measured by the change of the Dst index. In following section we analyse geomagnetic effect of CIRs that were recorded by *in situ* measurements at the Langrangian point L1, focusing on the period from January 2008 to December 2014. In particular, we focus on the Dst index as geomagnetic parameters to analyze in detail the relationship of four basic CIR related solar wind parameters: the magnetic field, B; the flow speed, v; the thermal proton speed, v_{th}; and proton density, Np, in different parts of CIRs, in front and behind the SI. In Section 2 we describe the data set used in this analyze. The data analysis is presented in Section 3, displaying the results for both analyzed parts of CIR. The main results and conclusions of the research are summarized and discussed in Section 4.

The data set

For measuring of solar wind disturbances at L1 point we used the data recorded by the Wind Magnetic Field Investigation (MFI) and Solar Wind Experiment (SWE) with 1 minute resolution data in GSE coordinates (http://wind.nasa.gov/mfi_swe_plot.php). For some SW disturbances we used aditional hourly-averaged level-2 data from ACE satellite (*Stone et al.,* 1998). Data is given at http://www.srl.caltech.edu/ACE/ASC/level2/. The CIR events were separated by detailed analysis of plasma and the magnetic field structure, as described in *Dumbović et al.* 2012. First we identified the increase of the plasma speed above the current background wind speed level, which corresponds to high-speed streams and were related to coronal holes (for details see *Vršnak, Temmer, and Veronig,*2007a). Then, we found the compression region or SI at the rising phase of the HSS from the data of plasma temperature, density and magnetic field (a sharp peak of the density and field strength, as well as sharp increase of temperature). With that data we were able to identify CIRs. For the analyzed period, from 283 solar wind disturbances, 216 have been recognized as a CIRs (76% of all SW samples). From the whole CIRs sample, 61% of CIRs show this typical field and plasma structure and SI inside the CIR can be clearly recognized. Between 216 CIR events, 43 events (15% of whole CIR sample) have complex signatures. Complex signatures are consequences of CIRs or ICME-CIR interactions. These events are are excluded in our analysis. List of CIRs are cataloged for general on the web page of Zagreb Observatory

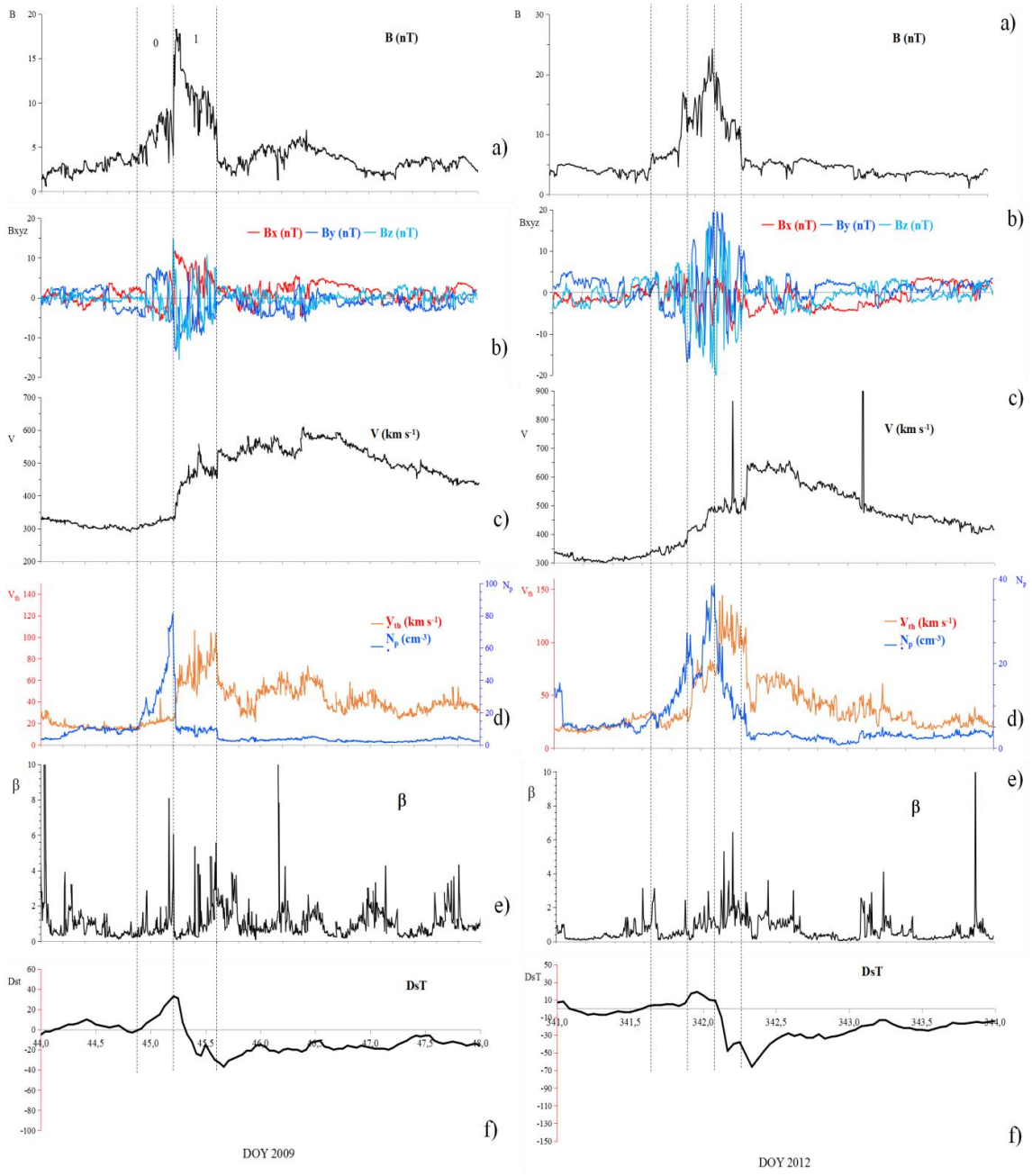

Figure 1. On both sides of presented figures the following labels are: a) the magnetic field strength, b) GSE magnetic field components, c) Theta and Phi magnetic field components d) solar-wind speed, e) proton density and thermal velocity f) plasma-to-magnetic pressure ratio and g) Dst index. Left form a) to g):Example of the CIR in situ WIND measurements at L1 (DOY (day of year) = 44 is 13 February 2009). This CIR, measured by WIND satellite occurred on 13 February 2009, represents events with clearly distinctive features of SI (middle dashed vertical line). The morphology of such CIR can be divided into two different parts: part of the CIR between the front wave and SI (which is marked with number 1) and part of the CIR between SI and reverse wave (which is marked with number 2). Right from a) to g): In situ Wind measurements at L1 (DOY = 341 is 6 December 2012). This CIR, measured by the WIND satellite 13 February 2009, shows events for which is not possible to clearly recognize the features of the SI. First and last vertical dashed line represent forward and reverse waves, while the two middle dashed lines represent two possible stream interfaces or interaction region.

(https://zvjezdarnica.hr/en/programs/science-and-scientific-work/exploring-of-the-icme/list-of-the-sirs-and-cirs/).

To exclude CIRs from ICMEs we also checked and compared with our own made database of ICMEs which can be found on the following link at (https://zvjezdarnica.hr/en/programs/science-and-scientific-work/exploring-of-the-icme/list-of-the-icmes/). For recognizing of the accompanied ICMEs we used data from STEREO satellites - SECCHI-COR2 Outer Coronagraph and SECCHI Heliospheric Imager (http://stereo-ssc.nascom.nasa.gov/browse/) SOHO satellite - LASCO C2 Coronagraph (http://lasco-www.nrl.navy.mil/daily_mpg/) and SDO Atmospheric Imaging Assembly (AIA) and Helioseismic Magnetic Imager (HMI) (http://sdo.gsfc.nasa.gov/data/). For the analyzed period we identified 1524 ICMEs. By simultaneously measuring the position angle (PA) in three coronagraphs, two COR2 from STEREO A & B and LASCO C2 chronograph from SOHO, we made a list of Earth directed ICMEs which have high probability to cause solar wind disturbance visible in solar wind data at 1 AU.

Furthermore, for every ICME we made elongation-time measurement, using HM approximation (developed by *Lugaz* 2010; for the application of the HM method see, *e.g*., *Möstl et al.* 2011, *Harrison et al.* 2012, *Rlloett et al.* 2012, and *Temmer et al.* 2012) we calculated the direction and arrival time of ICME at Earth distance. Using this simple method we correlated 105 ICMEs with 67 corresponding solar wind disturbances (24% of all SW disturbances). With this method it was possible to confirm is the CIR connected or affected with the arrival of the ICME. Solar wind signatures connected with the arrival of the ICME were excluded form our analysis.

We used the Dst index as the indicator of the geomagnetic activity (see *Rostoker,* 1972). The plasma and magnetic field data for the CIR were compared with Dst values we obtained from Kyoto University given at http://wdc.kugi.kyoto-u.ac.jp/dstdir/index.html. The geomagnetic disturbance index Dst (*Sugiura and Wilson,* 1964) represents the axially symmetric surface disturbance at the dipole equator of Earth, based on the hourly-averaged measurements of the horizontal magnetic field performed by four low latitude observatories. A decrease in Dst index is mainly caused by the ring current perturbation, while an weak increase in Dst is related to the compression of the magnetosphere caused by the increase in the solar wind dynamic pressure (frontal compression in the CIR).

Analysis

Correlation between Dst data with the solar wind *in situ* data, measured by WIND at L1, are shown in Figure 1. In Figure 1; in every plot the date is expressed as DOY. The *in situ* data in Figure 1 (left graphs) reveal the structure of the CIR, consists of two different parts (separated by vertical dashed lines). Middle vertical dashed line represents stream interface. In both parts we measured magnetic field strength, change in GSE magnetic field components, flow speed, maximum and minimum values of the flow speed components, temperature, proton density, plasma-to-magnetic field pressure (β) and change of Dst index. First region,

which we have marked with number 1 (part of the CIR between front wave and SI) is characterized by a gradual increase of magnetic field strength, decreased temperature, strong increase of proton density and increase of Dst index. Second region, which we have marked with number 2 (part of the CIR between SI and reverse wave) is characterized by a sharp drop of proton density, increased magnetic field strength, flow speed and temperature.

In Figure 1 (right graphs) the *in situ* - Dst data for the CIR signatures are recognized as events with complex signatures. As an example we take a CIR which arrives at L1 distance on 6 December 2012. For such CIRs it was not possible to clearly recognize the SI, but it was possible to recognize two or more SI, which can be casued by CIRs or ICME-CIR interaction. Those CIRs (43 events out of 216 CIRs for analyzed period, or 15% of whole CIRs semple) were excluded from further analysis. From Figure 1 (left), we concluded that in all CIRs with the "two part" structure, a weak positive increase of the Dst index occurs in the transition period for part 0 (between front wave and SI). The maximum Dst index is synchronized with SI, while the Dst index decrease occurs during the transition period of the part 1 (between SI and reverse wave). The results concerning the analyzed period (from January 2008 to December 2014) are presented in graphical form in Figures 2 - 4.

In Figures 2 we presented the scatter plots relating the change of Dst index (maximum minus minimum values) to the measured solar wind magnetic field strength, proton density, flow speed and temperature over the analyzed period. In Figures 2a-d we ploted solar wind data measured for part 0, while in Figure 2e-h we show measured values for region 1. The correlations for region 0 are very weak (cc = 0.57, 0.43, 0.18 and 0.56, respectively) and for region 1 are significantly higher (cc = 0.72, 0.62, 0.45 and 0.64, respectively).

Also, correlation for magnetic field strength and temperature are in both parts higher than correlations for proton density and flow speed. The graphs reveal a quite well defined lower and upper limits to Dst (B), Dst (Np), Dst (v) and Dst (v_{th}), indicated by the dotted line. There is no Dst activity for B in region 0 below 3 nT and in region 1 below 5 nT. Furthermore, there is no Dst activity for B in region 0 above 20 nT and in region 1 above 25 nT. In every graph we displayed the linear last-squares fit for Dst - solar wind parameter related data.

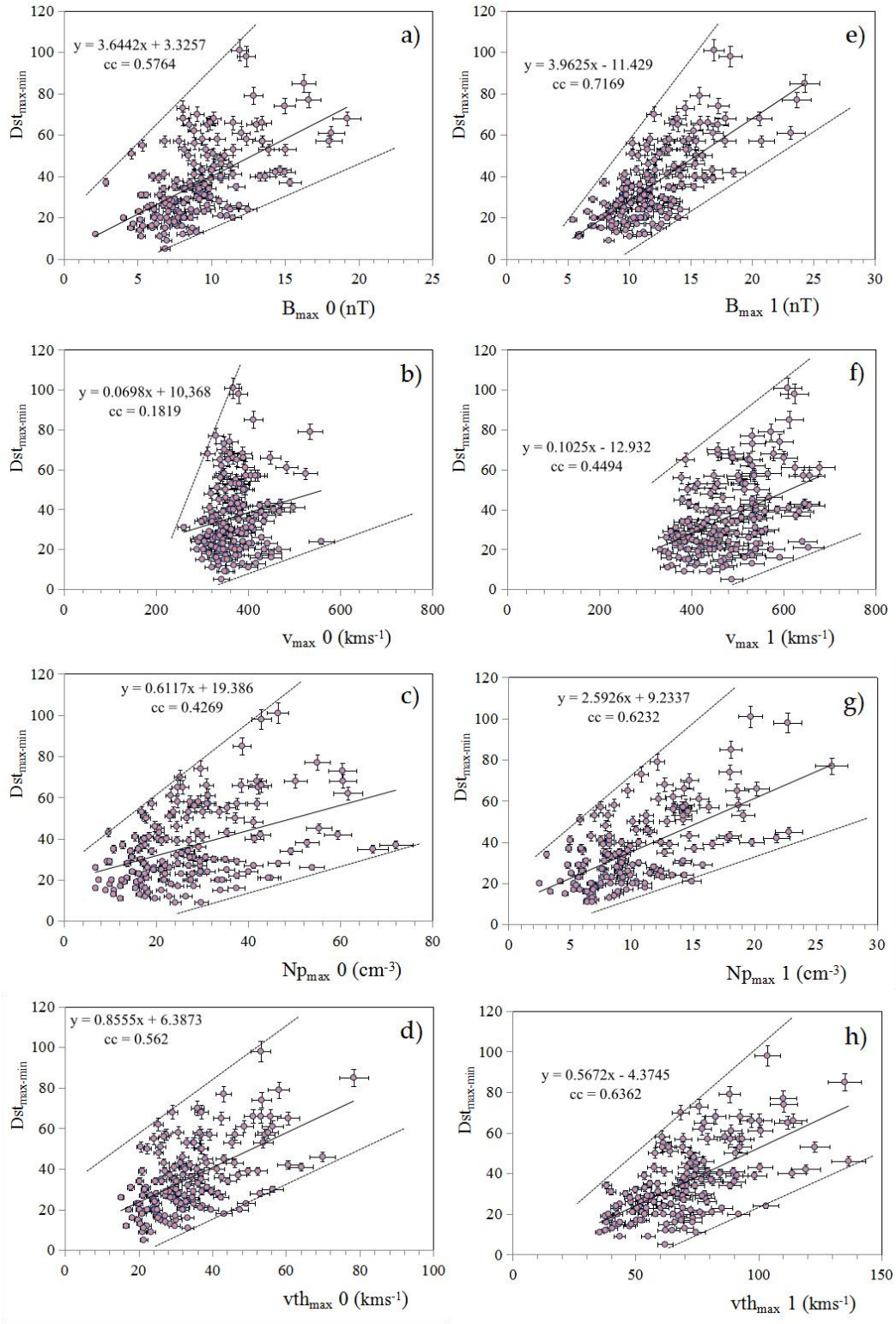

Figure 2. On both sides of presented figures the following labels are: a) the magnetic field strength, b) solar-wind speed, c) proton density and d) thermal velocity. Dashed line represents provisional drawn possible lower and heights values for the specific solar wind parameter. Variation of the Dst geomagnetic activity parameter (maximum - minimum values) versus four solar wind parameters measured in left for part 0 and right for part 1 (before SI, marked by 0).

Furthermore, because solar wind parameters show stronger correlations with Dst index in region 1, we made additional analysis of the GSE magnetic field and flow speed components for that region. In Figure 3a we presented the scatter plots of Dst index versus ΔB (difference between maximum of magnetic field strength in region 1 and 0). Also, in Figure 3b, c and d the scatter plots are given of Dst index versus variation of the CIR magnetic field components, B_x, B_y and B_z, in region 1. There are significant correlations for ΔB, B_x and B_z components, with correction coefficient of cc = 0.73, 0.58 and 0.68, respectively. A weak but significant correlation cc ~ 0.54 , was also found for B_y component.

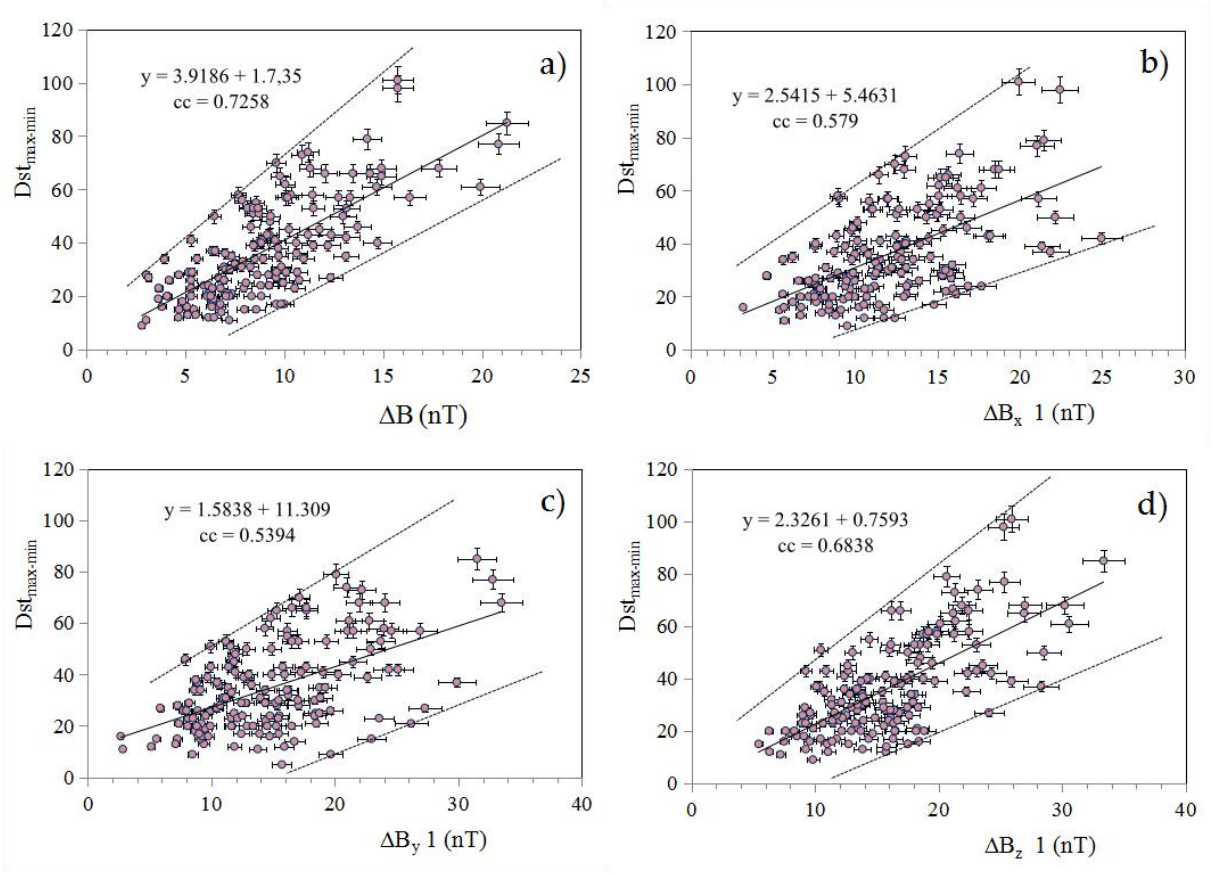

Figure 3. Variation of the Dst geomagnetic activity parameter versus ΔB - difference between maximum of magnetic field strength in region 1 and 0 (a), versus B_x (b), versus B_y (c) and versus B_z (d). Dashed line represents a provisional lower and heigher values for the specific solar wind parameter.

In Figure 4 we presented the dependence of the Dst versus Δv (difference between measured maximum of the flow speed in region 1 and 0), as well as variation (difference between measured maximum and minimum values) of the CIR flow speed components, v_x, v_y and v_z in region 1. The Figure 4 shows higher correlation between Δv and all flow speed components, but lower correlation between Δv and flow speed in both measured regions (Figure 2b and f). The correlation cc = 0.6 for Δv, is the highest correlation coefficient for Dst(v) of the CIR in both regions. Very weak correlation (cc = 0.46) was found for v_z

component of the flow speed in region 1, while for v_x and v_y the correlations are higher cc = 0.59 and 0.56, respectively.

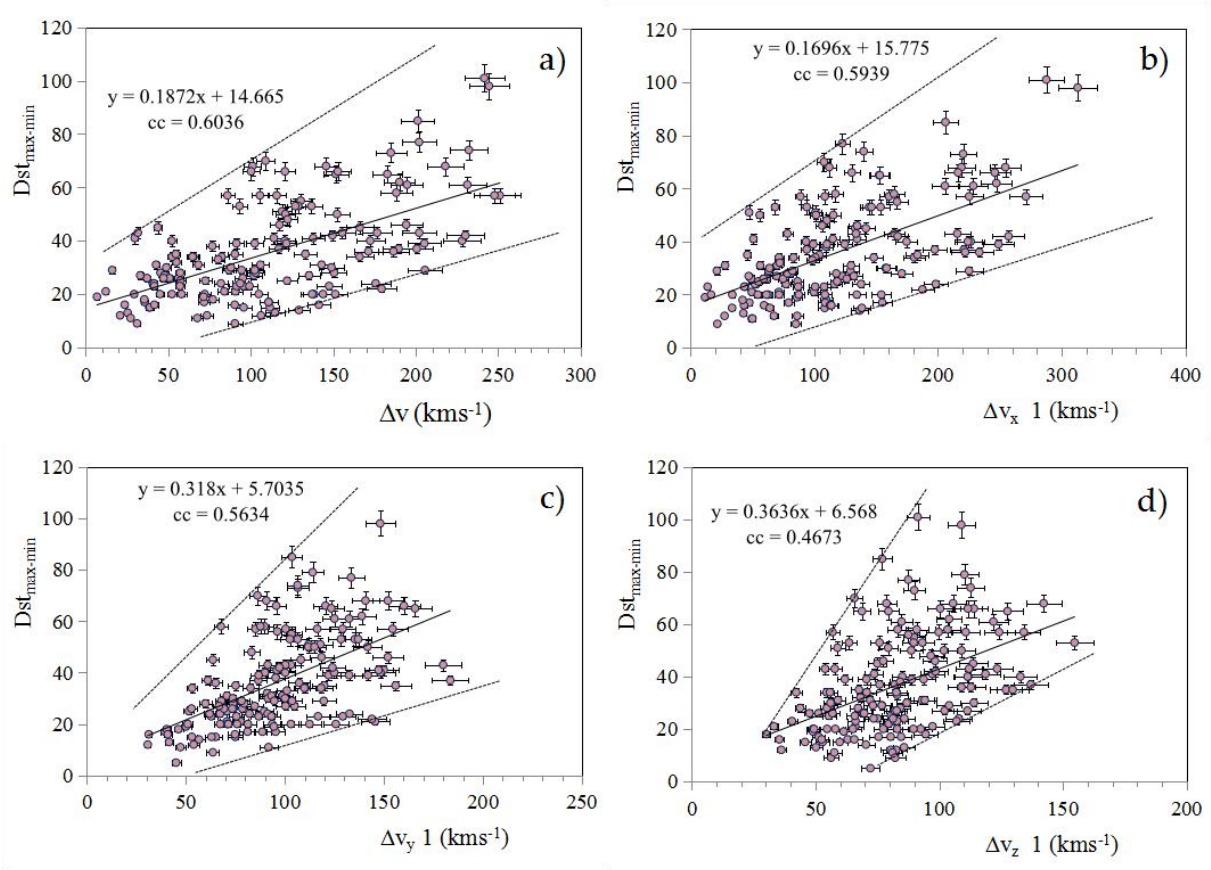

Figure 4. Variation of the Dst geomagnetic activity parameter versus Δv - difference between maximum of measured flow speed in region 1 and (a) 0, versus v_x (b), versus v_y (c) and versus vz (d) flow speed components. Dashed line represents a provisional lower and heigher values for the specific solar wind parameter.

Discussion and Conclusion

We summaries the main results of our analysis of the geoeffectiveness of two CIRs regions (before and after SI) as follows :

a) For 95% CIRs we analyzed, an increase of Dst index occurs between forward shock and SI (part marked as region 0), while the main decreases of Dst index occurs between SI and reverse shock of CIR (part marked as a region 1).

b)The correlation coefficients between the Dst index and the magnetic field *B*, proton density *N*p, flow speed *v* and proton thermal speed v_{th}, in the region behind the SI are: cc = 0.72, 0.62, 0.45 and 0.64, respectively.

c) Correlations for regions between forward shock and SI are significantly lower.

d) The correlation for magnetic field strength and temperature are in both regions higher than correlations for proton density and flow speed.

We would like to thank the WIND, ACE, SOHO, STEREO, SDO and Kyoto university teams for developing and operating the instruments and we are grateful for their open data policy.

References

Balogh, A., Gosling, J.T., Jokipii, J.R., Kallenbach, R., Kunow, H.: 1999, Corotating interaction regions.*Space Sci. Rev.* **89**, 1.

Dumbovicć, M., Vršnak, B., Čalogović, J., Župan, R.: 2012, Cosmic ray modulation by different types of solarwind disturbances. *Astron. Astrophys.* **538**, A28.

Gosling, J.T.: 1996, Corotating and transient solar wind flows in three dimensions. *Annu. Rev. Astron. Astrophys.***34**, 35.

Gosling, J.T., Pizzo, V.J.: 1999, Formation and evolution of corotating interaction regions and their threedimensional structure. *Space Sci. Rev.* **89**, 21.

Hajra, R., Echer, E., Tsurutani, B.T., Gonzalez, W.D.: 2013, Solar cycle dependence of high-intensity longdurationcontinuous AE activity (HILDCAA) events, relativistic electron predictors? *J. Geophys. Res.***118**, 5626.

Harrison, R. A., Davies, J. A., Möstl, C., Liu, Y., Temmer, M., Bisi, M. M., *et al*.: 2012, *Astrophys. J.* **750**, 45.

Lugaz, N.: 2010, *Solar Phys*. **267**, 411-429.

Möstl, C., Rollett, T., Lugaz, N., Farrugia, C.J., Davies, J. A., Temmer, M., *et al*.: 2011, *Astrophys. J.* **741**,34.

Rotter, T., Veronig, A.M., Temmer, M., Vršnak, B.: 2012, Relation between coronal hole areas on the sunand the solar wind parameters at 1 AU. *Solar Phys.* **281**, 793.

Rostoker, G.: 1972, Geomagnetic indices. *Rev. Geophys. Space Phys.* **10**, 935.

Smith, E.J., Wolfe, J.H.: 1976, Observations of interaction regions and corotating shocksbetween one andfive AU – Pioneers 10 and 11. *Geophys. Res. Lett.* **3**, 137.

Stone, E.C., Frandsen, A.M., Mewaldt, R.A., Christian, E.R.,Margolies, D., Ormes, J.F., Snow, F.: 1998, Theadvanced composition explorer. *Space Sci. Rev.* **86**, 1.

Sugiura, M., Wilson, C.R.: 1964, Oscillation of the geomagnetic field lines and associated magnetic perturbationsat conjugate points. *J. Geophys. Res.* **69**, 1211.

Temmer, M., Vršnak, B., Veronig, A.M.: 2007, Periodic appearance of coronal holes and the related variationof solar wind parameters. *Solar Phys.* **241**, 371.

Tsurutani, B.T., McPherron, R.L., Gonzalez, W.D., Lu, G., Sobral, J.H.A., Gopalswamy, N.: 2006, Introductionto special section on corotating solar wind streams and recurrent geomagnetic activity. *J. Geophys.Res.* **111**, 1.

Vennerstroem, S.: 2001, Interplanetary sources of magnetic storms: a statistical study. *J. Geophys. Res.* **106**,29175.

Verbanac, G., Vršnak, B., Veronig, A., Temmer, M.: 2011a, Equatorial coronal holes, solar wind high-speedstreams, and their geoeffectiveness. *Astron. Astrophys.* **526**, A20.

Verbanac, G., Vršnak, B., Živković, S., Hojsak, T., Veronig, A.M., Temmer, M.: 2011b, Solar wind high-speedstreams and related geomagnetic activity in the declining phase of solar cycle 23. *Astron. Astrophys.* **533**,A49.

Vršnak, B., Dumbović, M., Čalogović, J., Verbanec, G., Poljanić-Beljan, I.: 2017, Geomagnetic Effects of Corotating Interaction Region. *Solar Phys.* **292**, 140.

Vršnak, B., Temmer, M., Veronig, A.M.: 2007a, Coronal holes and solar wind high-speed streams: I. Forecastingthe solar wind parameters. *Solar Phys.* **240**, 315.